Lithium Storage Materials | Hot Paper

Deutsche Ausgabe: DOI: 10.1002/ange.201411353
Internationale Ausgabe: DOI: 10.1002/anie.201411353

Rutile TiO_2 Submicroboxes with Superior Lithium Storage Properties

*Xin-Yao Yu, Hao Bin Wu, Le Yu, Fei-Xiang Ma, and Xiong Wen (David) Lou**

Abstract: *Hollow structures of rutile TiO_2, and especially with non-spherical shape, have rarely been reported. Herein, high-quality rutile TiO_2 submicroboxes have been synthesized by a facile templating method using Fe_2O_3 submicrocubes as removable templates. Compared to other rutile TiO_2 nanomaterials, the as-prepared rutile TiO_2 submicroboxes manifest superior lithium storage properties in terms of high specific capacity, long-term cycling stability, and excellent rate capability.*

Hollow nanostructured metal oxides exhibit interesting electrochemical performance as electrode materials for lithium-ion batteries (LIBs) owing to the greatly enhanced diffusion kinetics and structural stability.[1–3] Up to now, various approaches have been developed to controllably synthesize different hollow nanostructured metal oxides.[1,4,5] Among these strategies, the hard-templating method has been demonstrated to be one of the most effective and conceptually straightforward strategies to achieve uniform, size-controllable, and well-defined hollow structured metal oxides.[4–11] These hard templates including silica, polymer latex, carbon nanospheres, and other colloidal particles are advantageous for narrow size distribution, ready availability in relatively large amounts, and simplicity of syntheses.[4,5] For example, using silica spheres as the template, we have synthesized coaxial carbon-coated SnO_2 hollow nanospheres that exhibit superior lithium storage capabilities.[12] Wang and co-workers reported the accurate synthesis of multi-shelled Co_3O_4 hollow microspheres as high-performance anode materials in LIBs by using carbonaceous microspheres as templates.[7] Although great advances have been achieved, the products obtained from template-engaged methods are mostly spherical in shape. Controllable synthesis of non-spherical hollow nanostructured metal oxides still suffer from many difficulties ranging from the paucity of available non-spherical templates to the challenge to form uniform coating around high-curvature surfaces.[1,4] Therefore, the design and synthesis of high-quality non-spherical hollow structured metal oxides, such as rutile TiO_2, still remain as a significant challenge until now.

Titanium oxide (TiO_2) materials are promising candidates as alternative electrode materials to carbonaceous anodes owing to their advantages in terms of low-cost, safety, and environmentally benign nature.[13–15] They can operate in conventional carbonate electrolytes with excellent stability and thus avoid the formation of solid electrode interphase (SEI) layers, owing to their high working voltage above 1 V vs. Li^+/Li.[13,16,17] The reversible lithium insertion has been demonstrated for many different TiO_2 polymorphs, including anatase, rutile, TiO_2(B), and brookite.[13,15,18–21] Among them, the rutile phase is most thermodynamically stable. Unfortunately, for a long time, rutile TiO_2 has been considered as a poor Li^+-insertion material owing to the limited Li^+ intercalation for bulk rutile.[22] At an elevated temperature of 120 °C, successful Li^+ insertion/extraction into microsized rutile particles using a lithium polymer cell has been demonstrated.[23] Recently, several reports have shown that nanosized rutile TiO_2 is more electroactive for lithium insertion at room temperature.[15,22,24–30] However, the lithium storage performance especially the long-term cycling stability of rutile TiO_2 is still unsatisfactory and needs to be further improved. On the other hand, nanoparticles tend to aggregate during the charge–discharge process, which largely hinders their practical applications. Compared with common nanoparticles, hollow nanostructures composed of nanosized primary building blocks could not only solve the problem of irregular aggregation, but also effectively shorten the transport path for both electrons and Li^+ ions in TiO_2 matrix and provide a large electrode/electrolyte contact area, which are expected to further improve the rate capability and cycling performance. However, so far, the preparation of hollow structured rutile TiO_2, especially with a non-spherical shape, remains unreported.

Herein, we report the successful synthesis of porous rutile TiO_2 submicroboxes for the first time by a facile templating method. When evaluated as anode materials for LIBs, these rutile TiO_2 submicroboxes manifest high specific capacity, long-life cycling stability, and excellent rate performance. The synthesis strategy of rutile TiO_2 submicroboxes is depicted in Figure 1. First, uniform Fe_2O_3 submicrocubes employed as the removable templates are coated with a conformal layer of TiO_2 by a newly developed solvothermal method to obtain Fe_2O_3@TiO_2 core@shell submicrocubes (step I). Next, the Fe_2O_3@TiO_2 core@shell submicrocubes are annealed in air to increase the crystallinity of the TiO_2 layer (step II). Finally, the Fe_2O_3 cores can be completely etched out to produce porous TiO_2 submicroboxes with entirely hollow interiors (step III).

Uniform Fe_2O_3 submicrocubes synthesized through a facile and scalable co-precipitation method[31] are employed

[*] Dr. X. Y. Yu, H. B. Wu, L. Yu, F. X. Ma, Prof. X. W. Lou
School of Chemical and Biomedical Engineering
Nanyang Technological University
62 Nanyang Drive, Singapore 637459 (Singapore)
E-mail: xwlou@ntu.edu.sg
davidlou88@gmail.com
Homepage: http://www.ntu.edu.sg/home/xwlou/
Dr. X. Y. Yu
Nano-materials and Environment Detection Laboratory
Hefei Institutes of Physical Science
Chinese Academy of Sciences, Hefei 230031 (PR China)

Supporting information for this article is available on the WWW under http://dx.doi.org/10.1002/anie.201411353.

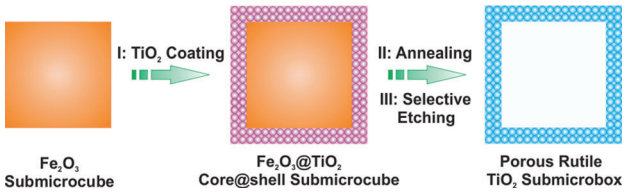

Figure 1. Illustration of the formation of porous rutile TiO_2 submicroboxes using Fe_2O_3 submicrocubes as templates. I: Fe_2O_3 submicrocube templates are uniformly coated with TiO_2 layer by an solvothermal method; II: the Fe_2O_3@TiO_2 submicrocubes are annealed in air to improve the crystallinity of TiO_2 layer; III: the Fe_2O_3 submicrocube templates are selectively removed by oxalic acid etching to obtain porous rutile TiO_2 submicroboxes.

as the template. Field-emission scanning electron microscopy (FESEM) images show that these Fe_2O_3 submicrocubes are highly uniform with an average size of around 500 nm (Figure 2a; Supporting Information, Figure S1a). X-ray powder diffraction (XRD) analysis confirms the successful

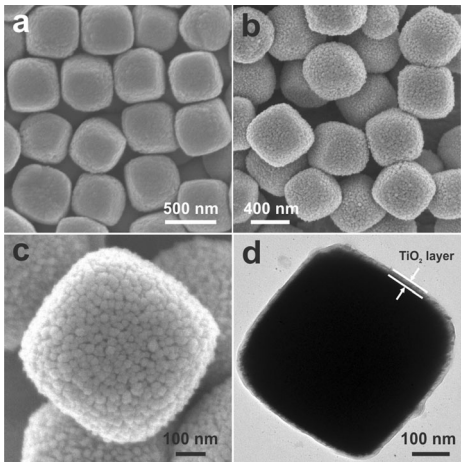

Figure 2. FESEM (a–c) and TEM (d) images of Fe_2O_3 submicrocubes (a) and Fe_2O_3@TiO_2 core@shell submicrocubes (b–d).

synthesis of α-Fe_2O_3 (Supporting Information, Figure S1b). Uniform TiO_2 shells are obtained in a diethylene glycol/acetic acid mixed solvent under solvothermal condition. The crystallographic structure of the as-prepared Fe_2O_3@TiO_2 core@shell submicrocubes is confirmed by XRD (Supporting Information, Figure S2). All of the peaks observed can be unequivocally assigned to rhombohedral hematite (JCPDS card no. 33-0664) and tetragonal rutile TiO_2 (JCPDS card no. 89-4202). Figure 2b–d show typical FESEM and transmission electron microscopy (TEM) images of the as-synthesized Fe_2O_3@TiO_2 core@shell structures. The increased roughness of these submicrocubes compared with the original Fe_2O_3 crystals (Figure 2b) indicates the formation of TiO_2 shells on the core particles. Figure 2c shows the FESEM image of a single Fe_2O_3@TiO_2 core@shell submicrocube displaying the cubic shape with a particulate surface. The core@shell structure is further confirmed by the low-magnification TEM image (Figure 2d), from which it is apparent that a thin TiO_2 layer has been coated on the whole surface of Fe_2O_3 core and the size of these Fe_2O_3@TiO_2 core@shell submicrocubes slightly increases to about 540 nm. The TiO_2 shells are quite uniform and thin (thickness of around 20 nm). After annealing treatment, the core–shell structure is well maintained without obvious alternation in morphology (Supporting Information, Figure S3).

The Fe_2O_3 template can be easily dissolved by oxalic acid, whereas TiO_2 is relatively stable in the solution, to obtain TiO_2 submicroboxes. As shown by XRD analysis (Supporting Information, Figure S2), a pure rutile phase is obtained without visible Fe_2O_3 residue. Compared with the TiO_2 layer in the Fe_2O_3@TiO_2 core@shell particles before annealing treatment, the crystallinity of TiO_2 submicroboxes is greatly improved. As shown in the low-magnification FESEM image in Figure 3a, the cubic structure is perfectly retained with an

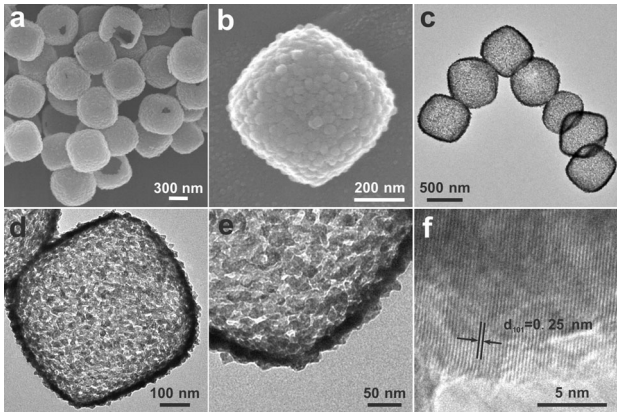

Figure 3. a), b) FESEM and c)–f) TEM images of porous rutile TiO_2 submicroboxes.

average size of about 540 nm. A close examination of a single TiO_2 submicrobox reveals a rough surface composed of TiO_2 nanoparticles (Figure 3b). The hollow interior and geometrical structure of the as-obtained TiO_2 submicroboxes are further elucidated by TEM (Figure 3c–e). In agreement with the above FESEM findings, the inner cavities can be clearly observed by the sharp contrast between the TiO_2 shell and hollow interior (Figure 3c,d). The shells of these submicroboxes are uniform and highly porous, with a thickness confirmed to be about 20 nm (Figure 3d). From the magnified TEM image of one corner of a single submicrobox (Figure 3e), it can be observed that the shell is constructed by nanoparticles with size of about 10–20 nm. Moreover, TEM images demonstrate the porous structure of these shells with pore size of several nanometers (Figure 3d,e). The lattice fringes in a typical high-resolution TEM image (Figure 3f) are separated by 0.25 nm, in good agreement with the (101) lattice spacing of rutile TiO_2. In virtue of the hollow structure and porous thin shell, the as-prepared rutile TiO_2 submicroboxes possess relatively high Brunauer–Emmett–Teller (BET) surface area of 57 $m^2 g^{-1}$ (N_2 adsorption–desorption isotherms are shown in the Supporting Information, Figure S4). The tap density of these rutile TiO_2 submicroboxes (0.44 $g cm^{-3}$) is much higher than that of P25 TiO_2 nanoparticles (0.17 $g cm^{-3}$).

To demonstrate the advantages of these TiO_2 submicroboxes, we investigated their electrochemical lithium storage properties as an anode material for LIBs. The cyclic voltammetry (CV) results (Supporting Information, Figure S5) are consistent with previously reported data.[30,32] The first cycle shows two cathodic peaks at about 1.4 and 1.0 V vs. Li/Li^+, which can be attributed to the lithium insertion into the rutile structure.[25,30,32] The peak current decreases significantly in the subsequent cycles, indicating the irreversible formation of $LiTiO_2$ phase from the rutile phase.[25,30,32] The CV curves of the second and fifth cycles almost overlap, demonstrating the good reversibility of the electrochemical reactions in the electrode after the first cycle.

Figure 4a shows representative discharge–charge voltage profiles of rutile TiO_2 submicroboxes at a current rate of 1 C within a cut-off window of 1.0–3.0 V. Consistent with the CV results, the first discharge curve shows two major poorly defined plateau regions at about 1.4 and 1.1 V vs. Li/Li^+, which agrees well with other nanosized rutile electrodes that have been reported.[22,24,33] The initial discharge process leads to a very high initial capacity of about 424 $mAh\,g^{-1}$, which greatly exceeds the theoretical capacity of rutile TiO_2 (335 $mAh\,g^{-1}$ for $Li^+ + e^- + TiO_2 \rightleftharpoons LiTiO_2$).[22,27] This is probably related to the hollow structure, which provides more surface active sites for lithium storage and other irreversible side reactions on nanosized rutile (for example, the above-mentioned irreversible reaction with residual water).[29,33] A lower capacity of 238 $mAh\,g^{-1}$ is obtained in the following charge process, leading to an irreversible capacity loss of 44%. The large irreversible capacity loss during the first cycle could be mainly related to the irreversible change of rutile structure between 1.4 and 1.0 V vs. Li/Li^+ for a deep lithium insertion.[22,24,25,33] The large volume strain induced during the lithium insertion causes the trapping of Li^+ ions inside the structure.[25] After the first cycle, the specific capacity of the TiO_2 submicroboxes electrode is stabilized. All the subsequent cycles show a slope profile of voltage-capacity relationship during both the charge and discharge processes (Figure 4a), which can be attributed to the formation of a nanocomposite of crystalline grains and amorphous regions.[15] A discharge capacity of 225 $mAh\,g^{-1}$ is delivered in the second cycle, followed by a charge capacity of 213 $mAh\,g^{-1}$, giving rise to a high Coloumbic efficiency (CE) of about 95%. The discharge capacity remains at about 188 $mAh\,g^{-1}$ after 200 cycles at a current rate of 1 C (Supporting Information, Figure S6). This performance is superior to most other nanostructured rutile TiO_2-based anode materials.[15,25,26,33–36] For comparison, irregular microparticles composed of rutile TiO_2 nanoparticles are also prepared by a similar method without the addition of Fe_2O_3 templates (Supporting Information, Figure S7), which exhibit inferior electrochemical activity (Supporting Information, Figure S6). Electrochemical impedance spectroscopy measurements demonstrate that TiO_2 submicroboxes show smaller diameter of high frequency semicircle than TiO_2 microparticles, indicating smaller solid-state interface resistance (Supporting Information, Figure S8).

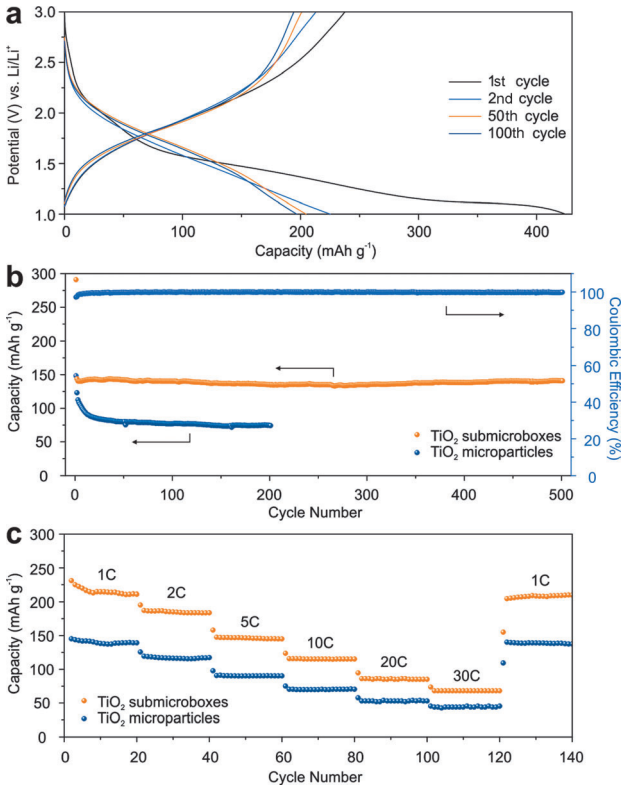

Figure 4. a) Charge–discharge voltage profiles of rutile TiO_2 submicroboxes for the 1st, 2nd, 50th, and 100th cycles at a current density of 1 C. (b) Cycling performance of rutile TiO_2 submicroboxes and TiO_2 microparticles at a current density of 5 C, and the corresponding Coulombic efficiency of rutile TiO_2 submicroboxes. c) Rate performance of rutile TiO_2 submicroboxes and TiO_2 microparticles at various current rates from 1 to 30 C. 1 C = 170 $mA\,g^{-1}$.

Moreover, the rutile TiO_2 submicroboxes can be cycled with high stability at higher current rates of 5 and 10 C (Figure 4b; Supporting Information, Figure S9). Remarkably, a reversible capacity of 141 $mAh\,g^{-1}$ at a current rate of 5 C after 500 cycles can still be retained with CE of almost 100% throughout the cycling. The excellent rate capability of the TiO_2 submicroboxes electrode is also investigated by charging and discharging at varying current rates ranging from 1 to 30 C (Figure 4c). Obviously, TiO_2 submicroboxes possess better cyclic stability and higher capacity than TiO_2 microparticles at each current rate. The average specific capacities for rutile TiO_2 submicroboxes are 210, 184, 146, 115, 85, and 68 $mAh\,g^{-1}$ at current rates of 1, 2, 5, 10, 20, and 30 C, respectively. Remarkably, after cycling at 30 C, a stable capacity of about 210 $mAh\,g^{-1}$ can still be delivered once the current rate is reduced back to 1 C, indicating the good structural stability of TiO_2 submicroboxes. TiO_2 submicroboxes with an average size of about 750 nm are also synthesized using larger sized Fe_2O_3 cores (700 nm) as templates (Supporting Information, Figure S10a,b). Similarly, the larger sized TiO_2 submicroboxes show comparable specific capacity and cycling performance (Supporting Information, Figure S10c).

The above results clearly evidence that hollow structured submicroboxes can greatly improve the electrochemical performance of rutile TiO_2 compared to the solid counterpart, which probably benefits from their unique structural charac-

teristics. Specifically, the high surface area of the hollow structure provides more active sites and electrolyte–electrode contact area for Li^+ insertion and surface lithium storage compared with solid counterparts. The small size of primary nanoparticles and the presence of permeable porous thin shells enable the much easier diffusion of Li^+ ions by shortening the transport length effectively. Meanwhile, the void space in the interior can accommodate large lattice distortion of the rutile TiO_2 upon Li^+ ions insertion/extraction, which will help maintain the structural integrity. With the enhanced structural stability and kinetics, lithium storage properties of the present TiO_2 submicroboxes are thus significantly improved.

In summary, we have developed a facile templating method for synthesizing porous rutile TiO_2 submicroboxes using Fe_2O_3 submicrocubes as removable templates. Uniform TiO_2 thin shells are first coated on Fe_2O_3 submicrocubes to form Fe_2O_3@TiO_2 core@shell structures. After subsequent removal of Fe_2O_3 cores with acid washing, high-quality rutile TiO_2 submicroboxes are obtained for the first time. Owing to the high surface area, porous thin shells, and small primary nanoparticles, these TiO_2 submicroboxes possess significantly improved lithium storage properties with remarkably stable capacity retention for over 500 cycles and enhanced rate capability at high rates up to 30 C.

Keywords: hydrothermal synthesis · lithium storage · nanostructures · rutile TiO_2 · submicroboxes

Zitierweise: *Angew. Chem. Int. Ed.* **2015**, *54*, 4001 – 4004
Angew. Chem. **2015**, *127*, 4073 – 4076

[1] Z. Y. Wang, L. Zhou, X. W. Lou, *Adv. Mater.* **2012**, *24*, 1903 – 1911.
[2] X. Y. Lai, J. E. Halpert, D. Wang, *Energy Environ. Sci.* **2012**, *5*, 5604 – 5618.
[3] H. B. Wu, J. S. Chen, H. H. Hng, X. W. Lou, *Nanoscale* **2012**, *4*, 2526 – 2542.
[4] X. W. Lou, L. A. Archer, Z. C. Yang, *Adv. Mater.* **2008**, *20*, 3987 – 4019.
[5] J. Hu, M. Chen, X. S. Fang, L. W. Wu, *Chem. Soc. Rev.* **2011**, *40*, 5472 – 5491.
[6] J. B. Joo, Q. Zhang, M. Dahl, I. Lee, J. Goebl, F. Zaera, Y. D. Yin, *Energy Environ. Sci.* **2012**, *5*, 6321 – 6327.
[7] J. Y. Wang, N. L. Yang, H. J. Tang, Z. H. Dong, Q. Jin, M. Yang, D. Kisailus, H. J. Zhao, Z. Y. Tang, D. Wang, *Angew. Chem. Int. Ed.* **2013**, *52*, 6417 – 6420; *Angew. Chem.* **2013**, *125*, 6545 – 6548.
[8] Z. Y. Wang, X. W. Lou, *Adv. Mater.* **2012**, *24*, 4124 – 4129.
[9] G. Q. Zhang, B. Y. Xia, C. Xiao, L. Yu, X. Wang, Y. Xie, X. W. Lou, *Angew. Chem. Int. Ed.* **2013**, *52*, 8643 – 8647; *Angew. Chem.* **2013**, *125*, 8805 – 8809.
[10] J. B. Joo, Q. Zhang, I. Lee, M. Dahl, F. Zaera, Y. D. Yin, *Adv. Funct. Mater.* **2012**, *22*, 166 – 174.
[11] Z. H. Dong, X. Y. Lai, J. E. Halpert, N. L. Yang, L. X. Yi, J. Zhai, D. Wang, Z. Y. Tang, L. Jiang, *Adv. Mater.* **2012**, *24*, 1046 – 1049.
[12] X. W. Lou, C. M. Li, L. A. Archer, *Adv. Mater.* **2009**, *21*, 2536 – 2539.
[13] G. N. Zhu, Y. G. Wang, Y. Y. Xia, *Energy Environ. Sci.* **2012**, *5*, 6652 – 6667.
[14] L. F. Shen, X. G. Zhang, H. S. Li, C. Z. Yuan, G. Z. Cao, *J. Phys. Chem. Lett.* **2011**, *2*, 3096 – 3101.
[15] Y. S. Hu, L. Kienle, Y. G. Guo, J. Maier, *Adv. Mater.* **2006**, *18*, 1421 – 1426.
[16] H. Kim, M. G. Kim, J. Cho, *Adv. Energy Mater.* **2012**, *2*, 1425 – 1432.
[17] L. M. Suo, S. Sallard, Y. S. Hu, B. M. Smarsly, L. Q. Chen, *ChemElectroChem* **2014**, *1*, 549 – 553.
[18] M. Anji Reddy, V. Pralong, U. V. Varadaraju, B. Raveau, *Electrochem. Solid-State Lett.* **2008**, *11*, A132 – A134.
[19] A. R. Armstrong, G. Armstrong, J. Canales, R. Garcia, P. G. Bruce, *Adv. Mater.* **2005**, *17*, 862 – 865.
[20] J. S. Chen, Y. L. Tan, C. M. Li, Y. L. Cheah, D. Y. Luan, S. Madhavi, F. Y. C. Boey, L. A. Archer, X. W. Lou, *J. Am. Chem. Soc.* **2010**, *132*, 6124 – 6130.
[21] S. H. Liu, Z. Y. Wang, C. Yu, H. B. Wu, G. Wang, Q. Dong, J. S. Qiu, A. Eychmuller, X. W. Lou, *Adv. Mater.* **2013**, *25*, 3462 – 3467.
[22] M. Pfanzelt, P. Kubiak, M. Wohlfahrt-Mehrens, *Electrochem. Solid-State Lett.* **2010**, *13*, A91 – A94.
[23] W. J. Macklin, R. J. Neat, *Solid State Ionics* **1992**, *53*, 694 – 700.
[24] C. H. Jiang, I. Honma, T. Kudo, H. S. Zhou, *Electrochem. Solid-State Lett.* **2007**, *10*, A127 – A129.
[25] J. S. Chen, X. W. Lou, *J. Power Sources* **2010**, *195*, 2905 – 2908.
[26] D. H. Wang, D. W. Choi, J. Li, Z. G. Yang, Z. M. Nie, R. Kou, D. H. Hu, C. M. Wang, L. V. Saraf, J. G. Zhang, I. A. Aksay, J. Liu, *ACS Nano* **2009**, *3*, 907 – 914.
[27] E. Baudrin, S. Cassaignon, M. Koesch, J. P. Jolivet, L. Dupont, J. M. Tarascon, *Electrochem. Commun.* **2007**, *9*, 337 – 342.
[28] W. J. H. Borghols, M. Wagemaker, U. Lafont, E. M. Kelder, F. M. Mulder, *Chem. Mater.* **2008**, *20*, 2949 – 2955.
[29] N. A. Milne, M. Skyllas-Kazacos, V. Luca, *J. Phys. Chem. C* **2009**, *113*, 12983 – 12995.
[30] M. A. Reddy, M. S. Kishore, V. Pralong, V. Caignaert, U. V. Varadaraju, B. Raveau, *Electrochem. Commun.* **2006**, *8*, 1299 – 1303.
[31] T. Sugimoto, Y. S. Wang, H. Itoh, A. Muramatsu, *Colloids Surf. A* **1998**, *134*, 265 – 279.
[32] P. Kubiak, M. Pfanzelt, J. Geserick, U. Hormann, N. Husing, U. Kaiser, M. Wohlfahrt-Mehrens, *J. Power Sources* **2009**, *194*, 1099 – 1104.
[33] B. T. Zhao, R. Cai, S. M. Jiang, Y. J. Sha, Z. P. Shao, *Electrochim. Acta* **2012**, *85*, 636 – 643.
[34] Z. S. Hong, M. D. Wei, T. B. Lan, G. Z. Cao, *Nano Energy* **2012**, *1*, 466 – 471.
[35] T. B. Lan, Y. B. Liu, J. Dou, Z. S. Hong, M. D. Wei, *J. Mater. Chem. A* **2014**, *2*, 1102 – 1106.
[36] B. Han, S. J. Kim, B. M. Hwang, S. B. Kim, K. W. Park, *J. Power Sources* **2013**, *222*, 225 – 229.

Received: November 23, 2014
Published online: February 4, 2015

